Implantation damage effects on the Er^{3+} luminescence in silica

T. Cesca,[1] C. Maurizio,[1] B. Kalinic,[1] G. Perotto,[1] P. Mazzoldi,[1] E. Trave,[2] G. Battaglin,[2] and G. Mattei[1,*]

[1]*Department of Physics and Astronomy, University of Padova, and CNISM, via Marzolo 8, I-35131 Padova, Italy*

[2]*Department of Molecular Sciences and Nanosystems, Ca' Foscari University of Venice, Dorsoduro 2137, I-30123 Venice, Italy*

[*]*giovanni.mattei@unipd.it*

Abstract: The possibility to control the room temperature Er^{3+} photoluminescence efficiency in silica is investigated in terms of the damage produced in Er-doped silica by implantations at different fluences with Xe or Au ions. These implantations are tailored to reproduce the same level of damage in Er-doped silica. The remarkable differences in terms of the photoluminescence intensity between Xe- and Au-irradiated samples allowed to decouple the detrimental effect of the implantation damage on the photoluminescence from the beneficial broad-band energy transfer process provided by molecule-like Au clusters formed upon thermal annealing. The evolution of the implantation damage is followed by photoluminescence and correlated to the local Er-site by x-ray absorption spectroscopy.

OCIS codes: (160.5690) Rare-earth-doped materials; (160.6030) Silica; (310.3840) Materials and process characterization; (260.2160) Energy transfer.

References and links

1. W. J. Miniscalco, "Erbium-doped glasses for fiber amplifiers at 1500 nm," J. Lightwave Technol. **9**, 234–250 (1991).
2. A. Polman, "Erbium implanted thin film photonic materials," J. Appl. Phys. **82**, 1–39 (1997).
3. A. Kenyon, "Recent developments in rare-earth doped materials for optoelectronics," Prog. Quantum Electron. **26**, 225–284 (2002).
4. F. Auzel, "Multiphonon-assisted anti-Stokes and Stokes fluorescence of triply ionized rare-earth ions," Phys. Rev. B **13**, 2809–2817 (1976).
5. C. Strohhöfer and A. Polman, "Absorption and emission spectroscopy in Er^{3+}-Yb^{3+}-doped aluminum oxide waveguides," Opt. Mater. **21**, 705–712 (2003).
6. M. Fuji, M. Yoshida, Y. Kanzawa, S. Hayashi, and K. Yamamoto, "1.54-μm photoluminescence of Er^{3+} doped into SiO_2 films containing Si nanocrystals: evidence for energy transfer from Si nanocrystals to Er^{3+}," Appl. Phys. Lett. **71**, 1198–1200 (1997).
7. G. Franzò, V. Vinciguerra, and F. Priolo, "The excitation mechanism of rare-earth ions in silicon nanocrystals," Appl. Phys. A **69**, 3–12 (1999).
8. D. Pacifici, G. Franzò, F. Priolo, F. Iacona, and L. Dal Negro, "Modeling and perspectives of the Si nanocrystals-Er interaction for optical amplification," Phys. Rev. B **67**, 245301 (2003).
9. F. Enrichi, G. Mattei, C. Sada, E. Trave, D. Pacifici, G. Franzò, F. Priolo, F. Iacona, M. Prassas, M. Falconieri, and E. Borsella, "Study of the energy transfer mechanism in different glasses co-doped with Si nanoaggregates and Er^{3+} ions," Opt. Mater. **27**, 904–909 (2005).
10. C. Strohhöfer and A. Polman, "Silver as a sensitizer for erbium," Appl. Phys. Lett. **81**, 1414–1416 (2002).
11. A. Martucci, M. de Nuntis, A. Ribaudo, M. Guglielmi, S. Padovani, F. Enrichi, G. Mattei, P. Mazzoldi, C. Sada, E. Trave, G. Battaglin, F. Gonella, E. Borsella, M. Falconieri, M. Patrini, and J. Fick, "Silver sensitized erbium doped ion exchanged sol gel waveguides," Appl. Phys. A **80**, 557–563 (2004).

#164874 - $15.00 USD
Received 16 Apr 2012; accepted 14 May 2012; published 9 Jul 2012

12. E. Trave, G. Mattei, P. Mazzoldi, G. Pellegrini, and C. Scian, "Sub-nanometric metallic Au clusters as efficient Er^{3+} sensitizers in silica," Appl. Phys. Lett **89**, 151121 (2006).
13. M. Mattarelli, M. Montagna, K. Vishnubhatla, A. Chiasera, M. Ferrari, and G. C. Righini, "Mechanisms of Ag to Er energy transfer in silicate glasses: a photoluminescence study," Phys. Rev. B **75**, 125102 (2007).
14. M. Eichelbaum and K. Rademann, "Plasmonic enhancement or energy transfer? on the luminescence of gold-, silver-, and lanthanide-doped silicate glasses and its potential for light-emitting devices," Adv. Funct. Mater. **19**, 2045–2052 (2009).
15. C. Maurizio, E. Trave, G. Perotto, V. Bello, D. Pasqualini, P. Mazzoldi, G. Battaglin, T. Cesca, C. Scian, and G. Mattei, "Enhancement of the Er3+ luminescence in Er-doped silica by few-atom metal aggregates," Phys. Rev. B **83**, 195430 (2011).
16. R. Espiau de Lamaestre, H. Béa, H. Bernas, J. Belloni, and J. L. Marignier, "Irradiation-induced Ag nanocluster nucleation in silicate glasses: Analogy with photography," Phys. Rev. B **76**, 205431 (2007).
17. J. Biersak and L. Haggmark, "A Monte Carlo computer program for the transport of energetic ions in amorphous targets," Nucl. Instrum. Meth. Phys. Res. B **174**, 257–269 (1980).
18. C. Maurizio, M. Rovezzi, F. Bardelli, H. G. Pais, and F. D'Acapito, "Setup for optimized grazing incidence x-ray absorption experiments on thin films on substrates," Rev. Sci. Instrum. **80**, 063904–1–6 (2009).
19. A. L. Ankudinov, B. Ravel, J. J. Rehr, and S. D. Conradson, "Real-space multiple-scattering calculation and interpretation of x-ray-absorption near-edge structure," Phys. Rev. B **58**, 7565–7576 (1998).
20. J. J. Rehr and R. C. Albers, "Theoretical approaches to x-ray absorption fine structure," Rev. Mod. Phys. **72**, 621–654 (2000).
21. F. d'Acapito, S. Mobilio, A. Terrasi, S. Scalese, G. Franzò, and F. Priolo, "Structure of Er-O complexes in crystalline Si," Phys. Rev. B **69**, 153310 (2004).
22. G. W. Arnold and P. Mazzoldi, in "Ion beam modification of insulators," , P. Mazzoldi and G. W. Arnold, eds. (Elservier, 1987), chap. 5.
23. E. Oliviero, M. Ruault, B. Décamps, F. Fotuna, E. Ntsoenzok, O. Kaïtasov, and S. Collin, "Synthesis of mesoporous amorphous silica by Kr and Xe ion implantation: Transmission electron microscopy study of induced nanostructures," Micropor. Mesopor. Mater. **132**, 163–173 (2010).
24. H. Haberland, B. von Issendorff, T. Kolar, H. Kornmeier, C. Ludewigt, and A. Risch, "Electronic and geometric structure of Ar_n^+ and Xe_n^+ clusters: The solvation of rare-gas ions by their parent atoms," Phys. Rev. Lett. **67**, 3290–3293 (1991).
25. A. Terrasi, G. Franzò, S. Coffa, F. Priolo, F. D'Acapito, and S. Mobilio, "Evolution of the local environment around Er upon thermal annealing in Er and O co-implanted Si," Appl. Phys. Lett. **70**, 1712–1714 (1997).
26. N. Gorbachuk, S. Kirienko, V. Sidorko, and I. Obushenko, *CRC Handbook of Chemistry and Physics* (CRC Press, 2005).
27. N. Gorbachuk, S. Kirienko, V. Sidorko, and I. Obushenko, "Thermodynamic properties of erbium mono-and disilicide at low temperatures," Powder Metallurgy Metal Ceram. **46**, 72–76 (2007).
28. C. Maurizio, F. Iacona, F. D'Acapito, G. Franzò, and F. Priolo, "Er site in Er-implanted Si nanoclusters embedded in SiO_2," Phys. Rev. B **74**, 205428 (2006).
29. P. Noé, H. Okuno, J.-B. Jager, E. Delamadeleine, O. Demichel, J.-L. Rouviere, V. Calvo, C. Maurizio, and F. D'Acapito, "The evolution of the fraction of Er ions sensitized by Si nanostructures in silicon-rich silicon oxide thin films," Nanotechnology **20**, 355704 (2009).
30. C. Piamonteze, A. C. Iñiguez, L. R. Tessler, M. C. Martins Alves, and H. Tolentino, "Environment of Erbium in a-Si:H and a-SiO_x:H," Phys. Rev. Lett. **81**, 4652–4655 (1998).
31. M. A. Marcus, D. Jacobson, A. Vredenberg, and G. Lamble, "Concentration and annealing effects on photoluminescence and local structure of Er-implanted silica," J. Non-Cryst. Solids **195**, 232–238 (1996).
32. J. Wan, Y. Ling, Q. Sun, and X. Wang, "Role of codopant oxygen in erbium-doped silicon," Phys. Rev. B **58**, 10415–10420 (1998).

1. Introduction

Er-doped silica-based materials are of strategic interest in the field of optical communication technology for their application as active elements in photonic devices. In particular, this is related to the sharp room temperature luminescent emission at 1540 nm of the Er^{3+} ions that matches the window of minimum loss in silica optical fibers. Nonetheless, the major limitation to the realization of efficient Er-based optical devices is given by the small cross-section for Er^{3+} excitation (typically of the order of 10^{-20} cm^2) [1–3]. To improve the rare-earth excitation efficiency, the interaction with fluorescence sensitizers, such as other rare-earth ions [4, 5], Si nanostructures [6–9] or metallic species [10–15] has been exploited.

As regards metal nanoparticles, the sensitization effect for the Er^{3+} luminescence has been

#164874 - $15.00 USD Received 16 Apr 2012; accepted 14 May 2012; published 9 Jul 2012

recently demonstrated for ultra-small Au nanoclusters (made by less than 20 atoms), incorporated in Er-doped silica matrices [12, 15]. In such experiments, ion implantation has been used to introduce both erbium and subsequently gold in the silica matrix. Post-implantation thermal treatments have been performed to recover the implantation-induced damage, to activate the Er luminescence and to promote the Au nanocluster formation.

An important point that is still open concerns the possible synergistic role of the defects induced by the subsequent Au implantation on the Er luminescence. Indeed, when the ion enters the substrate a wealth of complex defective and/or charged configurations are generated along the collisional cascade [16]. The physics and thermodynamics of such defects and their interactions under thermal annealing can largely influence the functional properties of the system. In particular, they could in principle affect both the rare-earth sensitization process and its luminescence quenching. The aim of the present work is therefore to investigate this aspect, by decoupling the sensitization mechanism triggered by the molecule-like Au clusters from the defects creation during Au implantation. For this reason, Er and Xe co-implantations have been performed following the same approach used to produce the Er-Au co-implanted samples investigated in Refs. [12, 15]. Xe has been chosen as co-dopant in order to release to the silica matrix an implantation damage as similar as possible to that induced by Au implantation. The Er^{3+} emission properties of the Er-Xe co-implanted samples have been characterized by integrated and time-resolved photoluminescence (PL) measurements and correlated to structural characterizations of the local environment around the Er centers obtained by extended x-ray absorption fine structure (EXAFS) spectroscopy.

2. Experimental

To prepare the samples, silica slabs (Herasil 1 by Heraeus) have been sequentially implanted with Er ions at three different energies (50, 100 and 190 keV), with a total fluence of $(6.6\pm0.9)\times10^{14}$ Er^+/cm^2, as measured by Rutherford Backscattering Spectrometry (RBS) using a 2 MeV $^4He^+$ beam. In this way, an almost flat, 70 nm thick, Er profile has been obtained with an Er concentration of about 10^{20} Er/cm^3 (that is below the threshold for concentration quenching of the Er emission [2]). After the Er implantation, thermal annealings at different temperatures in the range 300-1100 °C have been performed for 1h in N_2 atmosphere. The Er-implanted slab annealed at 800 °C has been subsequently implanted with Xe ions following the same triple energy scheme (50, 90 and 150 keV) to match the Er profile, at two different fluences, $(7.9\pm0.9)\times10^{14}$ Xe^+/cm^2 and $(7.8\pm0.9)\times10^{15}$ Xe^+/cm^2, respectively, as measured by RBS. The highest Xe^+ fluence was chosen to have an expected implantation damage on the Er-implanted silica similar to the one induced by the Au^+ implantation on the same system as in Ref. [12]. In that work the measured Au/Er concentration ratio was about 9. According to simulations obtained with the SRIM-2010 code [17], we evaluated that at the energies used in the present work the nuclear and electronic energy losses of Xe^+ in silica are about 30% lower than the corresponding quantities for Au^+ in silica. Therefore to better reproduce the implantation-induced damage we used a Xe^+ fluence about 30% higher with respect to the Au^+ one, resulting in a Xe/Er ratio of about 12. On the other hand, the lowest investigated Xe^+ concentration allowed to study the effect of an order of magnitude lower implantation damage on the Er^{3+} photoluminescence. Thus, the samples were labeled according to the level of damage induced by the Xe or Au implantations, i.e., HD (high damage) corresponds to a concentration ratio Er/Xe=1/12 (comparable to Er/Au=1/9) and LD (low damage) corresponds to Er/Xe=1/1.2.

Post Xe-implantation thermal treatments have been carried out for 1h in N_2 atmosphere in the temperature range 300-800 °C. The Er^{3+} emission properties at 1540 nm have been investigated by integrated and time-resolved photoluminescence measurements performed both with

#164874 - $15.00 USD Received 16 Apr 2012; accepted 14 May 2012; published 9 Jul 2012

resonant and not-resonant excitation, using, respectively, the 488 nm and 476.5 nm lines of a cw Ar laser mechanically chopped at 5 Hz.

The morphological and compositional characterization of the samples was performed in cross-section by transmission electron microscopy (TEM) with a FEI TECNAI F20 (S)TEM field-emission gun (FEG) microscope operating at 200 keV, equipped with an EDAX energy dispersive x-ray spectrometer (EDS) for compositional analysis and a scanning TEM (STEM) attachment with a high-angle annular detector for dark field STEM imaging (HAADF-STEM).

Er L_3-edge x-ray absorption spectra were recorded at the Italian beamline GILDA of the European Synchrotron Radiation Facility-ESRF (F) in fluorescence mode. The double crystal monochromator was equipped with two (111) Si crystals; the harmonics rejection was achieved by a couple of Pd-coated mirrors working at an incidence angle of 3.6 mrad. A grazing incidence geometry was used (incidence angle $\sim$2 deg) to increase the (low) fluorescence signal from Er, keeping at the same time the signal of the elastic scattering from the matrix as low as possible [18]. The x-ray absorption spectrum of Er_2O_3 crystalline powder was also measured in transmission mode as standard reference. The EXAFS analysis was performed with the FEFF8-FEFFIT package [19]: the Er-O and Er-Si backscattering amplitudes and phase shifts were calculated for $Er_2Si_2O_7$ and $ErSi_2$ clusters. The S_0^2 parameter of the standard EXAFS formula [20] was estimated by fitting the spectrum of the crystalline Er_2O_3. k^2-weighted EXAFS spectra were Fourier-transformed in the range k=2–8 Å^{-1} and the analysis was performed in the *R*-space. Since the first and the second coordination shells give rise to signals that partially overlap into the *R*-space (especially for low annealing temperature), the analysis was carried out in the R=1–4 Å range, i.e. considering altogether both the first and the second shell contributions, that are practically the whole EXAFS signal; the fit was based on the single scattering approximation; the use of multiple scattering paths did not lead to a significant improvement of the fit quality. As far as the first shell is concerned, as discussed in the following, in most of the cases a simple fit based on a single Er–O distance failed and an additional Er–Si coordination was needed to reasonably reproduce the experimental data. To fit the second shell we considered that O and Si atoms in the first shell are likely bonded to the silica matrix, i.e. to Si and O atoms, respectively; for this reason in the second coordination shell we have considered again a double population of O and Si atoms. We remark that for all the samples the main signal is due to O atoms in the first shell and Si atoms in the second one, that form a sort of Er silicate-like complexes. To reduce the number of fitting parameters, for the minor components of the signal, i.e. Si atoms in the first shell (Si^I) and O atoms in the second one (O^{II}), the ratio of the coordination numbers CN of the two shells $CN(Si^I)/CN(O^{II})$ was set the same for all the spectra. For the same reason, the same Debye-Waller factor was attributed to the two coordinations in the first shell (similarly for the second shell), estimated by the first shell fitting of the spectra from the 800 °C-annealed samples; this value (0.013 ± 0.002 Å^2) is pretty similar to the one obtained with full EXAFS spectrum analysis of the Er site in crystalline silicon [21]. In all cases the degrees of freedom in the fit were 4–5. A similar analysis performed on k^1- or k^3-weighted EXAFS spectra resulted less accurate but essentially in agreement with the first shell data presented in the following.

3. Results and discussion

In order to evaluate the effect of Xe implantation on the Er^{3+} emission properties, both the PL intensity at 1540 nm and the lifetime of the Er^{3+} emission of the Er+Xe co-implanted samples have been measured as a function of the annealing temperature and compared to the case without Xe implantation (i.e., Er implantation only). The results are shown in Fig. 1. For all the samples, the PL emission exhibited a single exponential decay which has been fitted to determine the lifetimes reported in the inset.

#164874 - $15.00 USD Received 16 Apr 2012; accepted 14 May 2012; published 9 Jul 2012

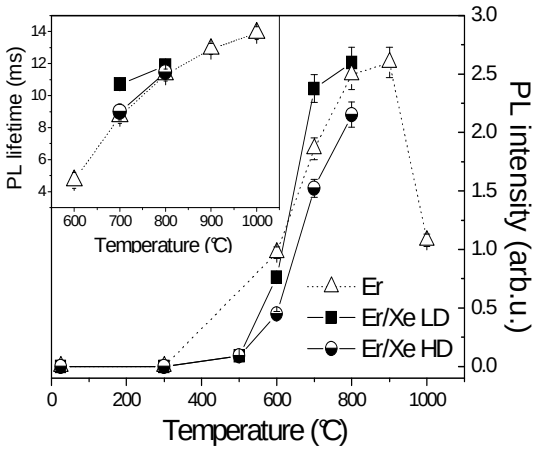

Fig. 1. PL intensity as a function of annealing temperature for the Er-implanted (white triangles) and the Er+Xe co-implanted samples (black squares for the Er/Xe LD and half-black circles for the HD samples, respectively). The measurements have been performed with resonant excitation at 488 nm. The inset shows the corresponding emission lifetimes. The legend is the same as for the PL intensity.

The evolution with the annealing temperature of the PL intensity of the samples implanted with Er only is reported in Fig. 1 as open triangles. In this case, no PL signal can be detected (within the sensitivity of our set-up) in the as-implanted and low temperature annealed samples. The onset of detectable PL emission occurs at temperatures above 600 °C and it starts to increase reaching a maximum value at 900 °C. For annealing at 1000 °C a further decrease of the PL intensity is observed. Correspondingly, the PL emission lifetimes (see inset) are characterized by a progressive increase in the whole temperature range, reaching values of about 12–14 ms which are typical of properly coordinated Er^{3+} emitting centers [2]. The onset of PL emission above 600 °C and the concomitant increase of PL intensity and lifetime in the 600–900 °C temperature range can be related to (i) a progressive recovery of the implant-induced defects in the silica matrix and (ii) to the formation of the full octahedral coordination of six oxygen atoms around the emitting Er^{3+} ion. Indeed, from one side, irradiation defects as dangling bonds, vacancy complexes or bond distortions in the glass [22] may act as nonradiative recombination centers giving rise to nonradiative decay processes involving energy transfer from the Er^{3+} ion towards acceptor states in the host and quenching the luminescent emission. On the other side, an incomplete oxygen shell (i.e., under-coordinated Er^{3+} ion) due to Er-O bond breaking and/or oxygen displacement under the collisional cascade can prevent a proper PL emission. After that the maximum PL intensity and lifetime is attained, the subsequent decrease of the PL signal observed at 1000 °C can be related to the onset of Er clustering phenomena that decrease the concentration of Er^{3+} active centers. Such clustering effect does not influence the lifetime that sightly increases due to a further recovery of the matrix defects.

As mentioned in the Experimental section, Xe implantations have been performed on silica slabs previously implanted with Er and annealed for 1h in N_2 atmosphere at 800 °C. For this annealing condition the Er-implanted samples exhibit a PL intensity close to its maximum value. Nonetheless, after Xe implantation at both investigated fluences such luminescent emission is completely suppressed and annealing treatments at temperatures above 600 °C are necessary to restore it. Moreover, the annealing evolution of the PL emission after Xe implantation at both fluences is comparable with the one measured from the Er-implanted samples, as shown in

#164874 - $15.00 USD
Received 16 Apr 2012; accepted 14 May 2012; published 9 Jul 2012

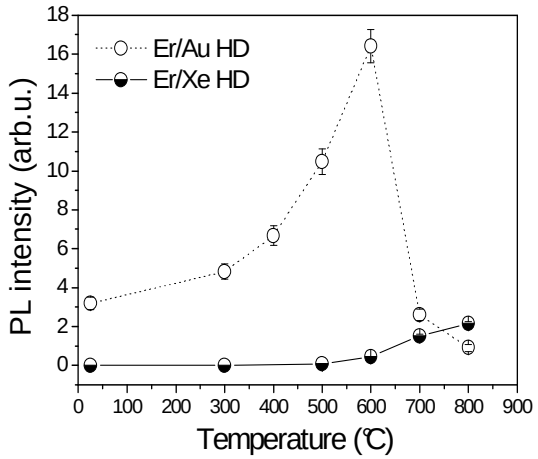

Fig. 2. Comparison of the temperature evolution of the PL intensity for the Er/Xe HD and Er/Au HD co-implanted samples under resonant excitation.

Fig. 1. An analogous behavior is observed also for the emission lifetimes (see inset in Fig. 1). In this case, only the samples annealed at the highest temperatures, that is 700 °C and 800 °C, exhibited a sufficiently intense luminescent emission to provide reliable estimations of the lifetimes from time-resolved PL measurements. For both fluences the measured lifetimes are close to those obtained in the Er-implanted samples. Only the Er/Xe LD co-implanted sample annealed at 700 °C exhibited a slightly longer lifetime with respect to the corresponding Er-implanted one, which can be ascribed to a reduced level of damage.

As a comparison, in Fig. 2 we have reported the PL intensity as a function of the annealing temperature for the Er/Xe HD and the Er/Au HD co-implanted samples under resonant excitation (488 nm). The results show the dramatically different temperature evolution exhibited by the Er+Au co-implanted samples with respect to that of Er+Xe co-implanted ones. In fact, in case of Er/Au HD co-implanted silica, the PL intensity is enhanced by the formation of very small Au aggregates (occurring up to T = 600 °C) that transfer part of the absorbed energy to the Er ions with a size-dependent efficiency (3–20 atoms clusters being the most efficient), as we showed in Refs. [12, 15]. Moreover, when the population of these efficient Au sensitizers is over (due to cluster growth, T>600 °C) the PL intensity decreases to values comparable to those of Er/Xe HD samples, in which the energy transfer process does not occur, as we will show below. This last result in particular allows to rule out the contribution of the implantation defects as the main source of energy transfer to Er^{3+} ions.

Indeed to get deeper information on the luminescent behavior of Er+Xe co-implanted samples, PL measurements have been also performed in out-of-resonance excitation condition (pumping with the 476.5 nm line of the Ar laser). The results are reported in Fig. 3(a), which shows the PL emission spectra around 1540 nm, both with resonant and not-resonant excitation, of the Er/Xe LD and Er/Xe HD co-implanted samples annealed at 800 °C. For both pumping conditions, the spectra of the Er-implanted sample annealed at 800 °C (that is the reference sample before Xe implantations) resulted very similar to those of the Er/Xe LD and HD co-implanted samples (annealed at the same temperature). Control measurements have been performed for all the samples implanted with Xe at both fluences and annealed at the different temperatures. With out-of-resonance excitation, no evidence of 1540 nm luminescent emission has been obtained independently of the annealing conditions and the Xe implantation fluences, i.e., independently of the implantation-damage level in the samples. This is a conclusive evidence

#164874 - $15.00 USD Received 16 Apr 2012; accepted 14 May 2012; published 9 Jul 2012

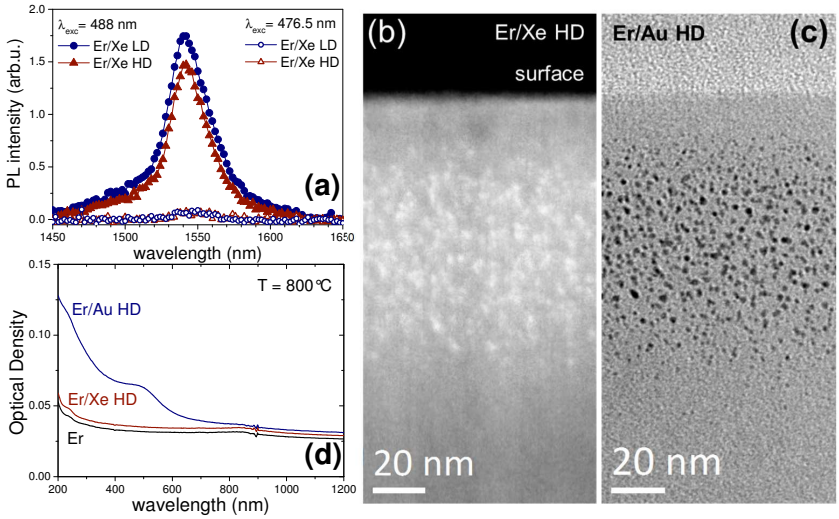

Fig. 3. (a) in-resonance (488 nm) and out-of-resonance (476.5 nm) Er^{3+} PL emission spectra around 1540 nm of the Er/Xe HD and LD samples annealed at 800 °C; (b) cross-sectional HAADF-STEM image of the Er/Xe HD sample annealed at 800 °C; (c) BF-TEM cross section of the Er/Au HD sample annealed at 800°C; (d) comparison of the optical absorption spectra of the samples annealed at 800°C.

of the absence of any energy transfer process (at the explored excitation wavelengths) in the Xe-implanted samples, contrary to what was found for the Au-implanted samples. Therefore, the present result further supports the conclusion that molecule-like Au clusters are required to achieve a broadband energy transfer to Er^{3+} ions [12, 15].

We would like to stress the structural and morphological similarity between Xe-implanted and Au-implanted Er-codoped silica. Figure 3(b) shows the cross-section image of the Er/Xe HD sample annealed at 800 °C taken in STEM high-angle annular dark field (HAADF-STEM) mode. In this technique the image contrast is proportional to the atomic number therefore the bright spots below the surface can be interpreted as Xe clusters (bubbles) with size of about 2 nm. No lattice fringes can be obtained in high-resolution mode (HR-TEM) nor diffraction rings in electron diffraction. This is an indication that the Xe aggregates are amorphous clusters or gas bubbles. Indeed, large Xe bubbles can be formed in silica under high fluence Xe implantation [23], e.g., above 10^{16} ions/cm^2 . Their formation is generally attributed to the low solubility of noble gas atoms which therefore tend to segregate in the damaged silica. This relatively low solubility of Xe is also typical of Au in silica. For comparison, Fig. 3(c) shows the bright-field (BF-TEM) cross section image of the sample Er/Au HD annealed at the same temperature. Crystalline spherical Au nanoclusters were detected with size 1.6 ± 0.5 nm , i.e., very similar to that of the Xe bubbles of the Er/Xe HD sample.

Xenon in form of dispersed atoms or as a neutral cluster is not expected to have specific absorption or emission bands in the VIS-NIR region [24]. On the contrary, charged Xe_n^+ clusters can have (size-dependent) absorption bands close to 1.5 eV, 2 eV and 3 eV, as shown for $n \leq 30$ free cationic clusters [24]. We did not find evidence of Xe-related absorption bands, in particular close to the excitation wavelengths used in the present works (476.5 nm and 488 nm): in Fig. 3(d) a comparison between the absorption spectra of the Er/Xe HD and Er/Au HD annealed at 800°C is reported. While the Er/Xe HD sample exhibits an absorption spectrum very similar to the pure Er reference sample, in the Er/Au HD the onset of the interband transitions

#164874 - $15.00 USD
Received 16 Apr 2012; accepted 14 May 2012; published 9 Jul 2012

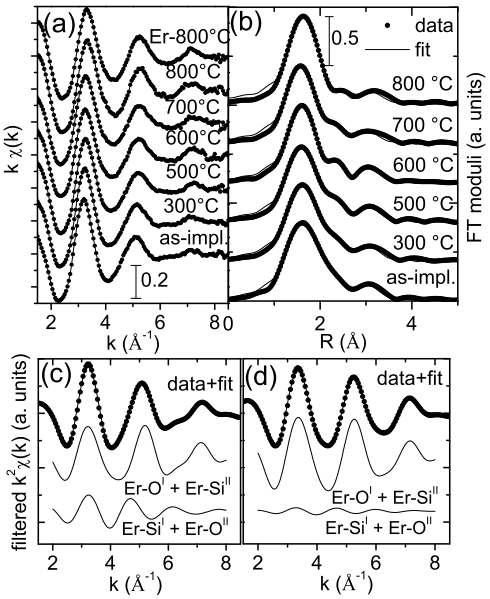

Fig. 4. (a) EXAFS spectra of the Er/Xe HD co-implanted samples, compared to the spectrum of an Er-implanted silica annealed at 800 °C; (b) k^2-weighted Fourier transform (in the range k=2–8 Å^{-1}) moduli (markers) and fits (solid line) of the spectra in (a); in (a,b) the annealing temperature is reported. (c,d) Fourier-filtered (in the range R=1–4 Å) signal (markers) superimposed to the best fit curve (solid line) for the as-implanted (c) and 800 °C-annealed samples (d); the signals that contribute to the fit are also reported (O in the first shell + Si in the second one and Si in the first shell + O in the second one).

absorption and of the surface plasmon resonance of small Au nanocluster is clearly visible. At lower annealing temperatures, Er/Xe HD samples do not exhibit major differences with respect to the optical absorption of the 800 °C-annealed ones.

Despite the close similarity between Er/Xe HD and Er/Au HD samples in terms of both damage produced and clustering of the implanted species, the effect on the energy transfer process is dramatically different as shown in Fig. 2. Moreover, the PL results indicate that the defects induced in the silica matrix by the Xe implantations behave as nonradiative de-excitation channels for the Er^{3+} emission as well as those produced by the Er implantation itself. Similar post-implantation treatments are needed to restore the luminescent properties of the samples, independently of the implantation fluence, at least in the range explored in this work.

To investigate the nature of the implantation induced damage on the Er site, we performed EXAFS analysis at the Er absorption edge to correlate the above PL results with the evolution of the local atomic structure around Er ions. The EXAFS spectra of the Er/Xe HD co-implanted samples are reported in Fig. 4(a) and compared with the spectrum of an Er-implanted silica annealed at 800°C; in Fig. 4(b) the Fourier transform (FT) moduli are shown together with the best fit curves. For all the samples, the EXAFS signal (Fig. 4(a)) -damped at high k values- is typical of a light backscatterer, i.e., mainly oxygen in this case. The EXAFS spectra show some differences in the k=5.5–8 Å^{-1} region: in particular, in this range the signal of the as-implanted sample is very low, while it progressively increases at higher annealing temperatures. Correspondingly, the main peak of the Fourier transform modulus related to the Er-O coordination (Fig. 4(b)) is highly asymmetric for the as-implanted sample, while the shoulder on its

#164874 - $15.00 USD
Received 16 Apr 2012; accepted 14 May 2012; published 9 Jul 2012

Table 1. Results of the EXAFS analysis for the first shell for Er and Er/Xe HD samples; *N* is the coordination number, *R* the interatomic distance. The Debye Waller factor σ^2 has been set to $(13 \pm 2) \times 10^{-3}$Å^2 for all the samples and for both O- and Si-coordination, as estimated by the first shell fitting of the spectra from the 800 °C-annealed samples

sample	T (°C)	O coordination (first shell) N	O coordination (first shell) R (Å)	Si coordination (first shell) N	Si coordination (first shell) R (Å)
Er/Xe HD	-	4.9 ± 0.6	2.18 ± 0.02	1.8 ± 0.5	2.69 ± 0.04
”	300	4.8 ± 0.6	2.18 ± 0.02	1.5 ± 0.5	2.71 ± 0.04
”	500	4.7 ± 0.6	2.16 ± 0.02	1.3 ± 0.5	2.72 ± 0.04
”	600	4.9 ± 0.6	2.16 ± 0.02	1.0 ± 0.5	2.79 ± 0.04
”	700	4.9 ± 0.6	2.14 ± 0.03	1.0 ± 0.7	2.72 ± 0.07
”	800	5.7 ± 0.6	2.17 ± 0.02	0.5 ± 0.6	2.84 ± 0.09
Er	800	5.6 ± 0.6	2.17 ± 0.02	0.4 ± 0.5	2.79 ± 0.06

right-hand side (at R≈2–2.5 Å) progressively fades at higher temperature leading to an almost symmetric peak upon annealing at 800 °C. These observations can be quantified only if a full analysis extended up to at least k=8.0 Å^{-1} is performed and for relatively low-noise data.

To properly fit the first shell EXAFS signal, including the shoulder discussed above, two different coordinations have to be considered: in fact, the use of an asymmetric distance distribution alone failed to reproduce the experimental data. The shorter coordination is the dominant signal and comes from the nearest O shell; the second one is responsible for the right-hand side shoulder of the first peak in the Fourier transform moduli, and is related to a light backscatterer, such as Si and/or O. This signal is a minor part of the whole first shell contribution to the EXAFS spectrum, so the data analysis alone could not lead to strong conclusive arguments about the nature of the backscatterer (O or Si, or even a coexistence of both). Nevertheless, we remark that: (i) this second contribution to the first shell is thermodynamically unstable and vanishes at high annealing temperature and (ii) the ion implantation process determines a depletion of O atoms in the implanted region, so that the formation of dopant-Si bonds is favored. For these reasons, this contribution to the first shell is more likely due to Si atoms. Similarly to this case, it has been shown that the local site of Er ions co-implanted with O in crystalline Si exhibit a main Er–Si coordination that is progressively substituted by the more stable Er–O coordination upon annealing [25] (as a comparison, the heat of formation ΔH_f of Er_2O_3 is 1898 kJ/mol [26], to be compared with ∼85 and ∼63 kJ/mol of ErSi and $ErSi_2$, respectively [27]). Another fact that supports this picture is that a first attempt to fit the first shell experimental data with O atoms at two different distances led to a Debye-Waller factor higher for the spectra of the samples annealed at higher temperature, that is unlikely to happen.

About the second shell, it is known that Er atoms bonded to O atoms embedded into silicon, silicon oxide and silica-based matrix exhibit a second shell coordination of Si atoms of the matrix [21,28,29]; in the present case, we consider that O atoms (Si atoms) in the first shell are likely bonded to Si atoms (O atoms) of the matrix, with the result that the second coordination shell (signal in the range R = 2.7–4 Å) is formed of both Si and O backscatters, connected to Er ions via O and Si species, respectively. In Fig. 4(c) and 4(d) data and fit are shown in the Fourier-filtered *k*-space for the as-implanted and 800 °C-annealed samples, respectively; the main signal from O in the first shell (+ Si in the second one, $Er–O^{I}$+$Er–Si^{II}$) and the minor contribution from Si in the first shell (+ O in the second one, $Er–Si^{I}$+$Er–O^{II}$) are reported

#164874 - $15.00 USD Received 16 Apr 2012; accepted 14 May 2012; published 9 Jul 2012

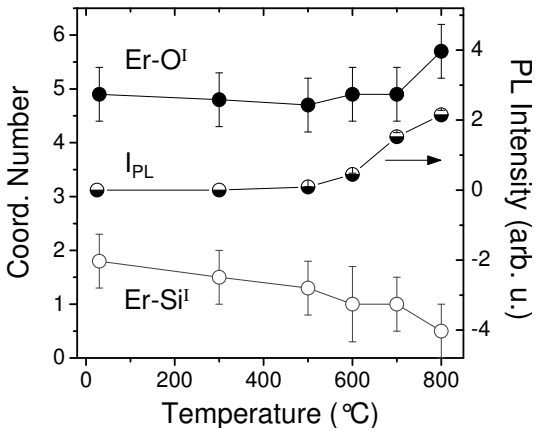

Fig. 5. First shell coordination number for the Er–O^I and Er–Si^I components as a function of the annealing temperature in the sample Er/Xe HD (left axis). On the right axis, the evolution of the Er/Xe HD photoluminescence intensity I_{PL}.

in the two cases: it is evident that the contribution from Er-Si^I+Er–O^{II} coordination becomes negligible upon high temperature annealing.

For the first shell, the results of the EXAFS analysis are reported in Table 1. For the as-implanted Er/Xe HD sample, the average Er site is composed of about 5 O atoms and about 2 Si atoms. The Er–O distance is significantly shorter than in the Er_2O_3 and $Er_2Si_2O_7$ crystals (where R = 2.23–2.31 Å), but is in the range of distances usually observed in Er-doped silica-based systems [28, 30, 31] especially when the preparation conditions are far from equilibrium. Moreover, the Er–Si distance is significantly shorter than in Er-silicide crystals (that is about 3.00 Å in $ErSi_2$, 2.80–3.17 Å in ErSi); nevertheless, theoretical analysis on Er+O-doped crystalline Si indicates Er–O and Er–Si first shell distances of 2.18 Å and 2.60 Å, respectively, similar to the value found in the present case [32]. Upon annealing, the number of O atoms in the first shell slightly increases, and Er ions reach practically the full octahedral coordination, i.e. the standard six-fold coordination of Er^{3+} in crystals, upon annealing at T = 800 °C; correspondingly, the number Si atoms in the first shell significantly decreases and becomes negligible upon annealing at 800 °C (see Figs. 4(d) and 5). So, the presence of both Si and O atoms in the first shell, observed upon annealing at T $<$ 800 °C likely suggests that the electronic configuration around the Er site may be different from that of Er ions octahedrally coordinated with just O atoms.

As far as the signal from the second coordination is concerned, the analysis indicates that, on the average, the second shell of atoms surrounding Er ions is composed of 3–5 Si atoms and a number of O atoms that, being linked to the first Si coordination (see details in the Experimental section), from about 3 progressively vanishes by increasing the annealing temperature. In all cases the Er–Si^{II} distance is 3.7 $\pm$0.1 Å, similar to what found in Er+O-implanted crystalline silicon [21], while the Er–O^{II} distance is 3.1$\pm$0.1 Å. Moreover, the EXAFS signals of the two samples annealed at 800 °C, i.e. with and without Xe implantation, are identical (see Fig. 4(a) and Table 1). These results indicate that the Er-Si coordination in the first shell is related to the defects formed upon Xe implantation: at high temperature annealing the matrix and the Er site recover from radiation damage and, correspondingly, the Er–Si coordination vanishes and only the octahedral coordination with O atoms remains.

It is worth noting that the EXAFS results for the Er/Xe LD as-implanted sample are very similar to those of the Er/Xe HD as-implanted sample indicating that, within the EXAFS sensi-

#164874 - $15.00 USD
Received 16 Apr 2012; accepted 14 May 2012; published 9 Jul 2012

tivity, the Er site does not depend on the Xe implantation fluence, at least for the fluence range explored in this work.

In Fig. 5 the thermal evolution of the Er–O^I and Er–Si^I coordination numbers in the first shell are plotted together with the PL intensity for the Er/Xe HD sample. A good direct correlation between PL efficiency and the Er–O^I is shown, indicating that the main contribution to the PL intensity comes from a properly structured Er^{3+} environment, i.e., when the fully octahedral configuration of the oxygen atoms around each erbium ion is reconstructed by the thermal annealing, with the consequent fading of the Er–Si^I contribution, the Xe-implanted Er-doped silica recoveries a PL efficiency (both intensity and lifetime) very similar to the nonimplanted Er reference sample.

4. Conclusion

We investigated the thermal evolution of the Er^{3+} PL emission in silica under the influence of implantation with Xe ions at different fluences. In particular we found that Xe implantation is remarkably different with respect to an equivalent Au implantation that is carried out so as to release approximately the same level of implantation damage. In particular, Xe is not able to produce energy transfer to Er^{3+} under non-resonant excitation, at variance with the Au case, despite the close similarity in terms of the size of the precipitates evidenced by TEM under Xe- or Au-implanted samples. This result clearly demonstrates that the energy transfer responsible for out-of-resonance excitation of Er^{3+} cannot be ascribed to implantation induced defects but is actively triggered by ultra-small molecule-like Au clusters, which absorb the non-resonant excitation and efficiently transfer it to Er^{3+} emitting centers.

To confirm this picture, we followed the evolution of the Xe implantation-induced damage around the Er^{3+} site in silica. EXAFS analysis demonstrated the presence of two different short-range coordinations in the Er site: one Er–O coordination at R = 2.14–2.18 Å, that is in the typical range of distance for Er^{3+} in silica, and one longer coordination with Si atoms at R = 2.7–2.8 Å. In particular the Er–Si coordination progressively fades as the annealing temperature is raised. A second coordination shell indicates that O and Si atoms in the first shell are further bonded with the matrix network. The monotonic increase of the PL intensity as a function of the annealing temperature in the Xe-implanted samples is found to be correlated to the increase of the Er–O coordination number and to the decrease of the Er–Si coordination, suggesting that these two configurations greatly affect the Er emission efficiency recovery.

Acknowledgments

We acknowledge Francesco d'Acapito (CNR-IOM c/o GILDA-ESRF, Grenoble-F) for fruitful discussion; the European Synchrotron Radiation Facility and the Italian Collaborating Research Group for the provision of the synchrotron radiation facility. GILDA is a project jointly financed by CNR and INFN. This work has been partially supported by the Progetto di Ateneo CPDA101587 of the University of Padova, Italy.

#164874 - $15.00 USD Received 16 Apr 2012; accepted 14 May 2012; published 9 Jul 2012